Research Article | Vol. 29, No. 8 / 12 April 2021 / Optics Express 11406

Optics EXPRESS

Distinction of electromagnetically induced transparency and Autler-Towners splitting in a Rydberg-involved ladder-type cold atom system

ZHONGHUA JI,[1,2,3] YUECHUN JIAO,[1,2] YONGMEI XUE,[1,2] LIPING HAO,[1,2] JIANMING ZHAO,[1,2,4] AND SUOTANG JIA[1,2]

[1] *State Key Laboratory of Quantum Optics and Quantum Optics Devices, Institute of Laser Spectroscopy, Shanxi University, Taiyuan 030006, China*
[2] *Collaborative Innovation Center of Extreme Optics, Shanxi University, Taiyuan, Shanxi 030006, China*
[3] *jzh@sxu.edu.cn*
[4] *zhaojm@sxu.edu.cn*

Abstract: Electromagnetically induced transparency (EIT) and Autler-Townes splitting (ATS) are two similar quantum coherent phenomena but have different mechanisms and applications. Akaike information criteria (AIC), an objective method to discriminate EIT and ATS from an experimental viewpoint, has been employed in a variety of systems. Here we use AIC method to quantitively discriminate a series of spectra of cold atoms in a Rydberg-involved upper-driving ladder-type. The derived weights of EIT and ATS reflect that our spectra change from EIT-ATS intermediate region to ATS-dominated region along Rabi frequency of coupling field increases. We find that there are two factors affecting EIT-ATS weights in a Rydberg-involved three-level system: dephasing rate, induced by the interactions among Rydberg atoms, makes the EIT-ATS crossover move to the direction of low Rabi frequency of coupling field and the experimental noise makes the difference between EIT and ATS weights reduce at elsewhere. Our investigation could provide a meaningful reference for the observations and applications of Rydberg-involved quantum coherent spectroscopy.

1. Introduction

Electromagnetically induced transparency (EIT) is a quantum interference phenomenon in which the transmission of a weak probe field is enhanced in the presence of a strong (near-)resonant coupling field [1–3]. Arising from the destructive Fano interference [4], EIT has exhibited numerous applications, such as lasing without inversion [5], high-precision magnetometry [6], slow light propagation [7], light storage [8] and quantum transistor [9]. Another similar but different quantum coherent phenomenon is Autler-Townes splitting (ATS) [10], in which a linear a.c. Stark effect is caused by the strong coupling field and then the induced dressed states are measured by the weak probe field. Without interference characteristic, applications of ATS are mainly limited in spectroscopy-based measurements, like transition dipole moment [11] and lifetime [12], along with very few exploration utilizing quantum coherence (to our knowledge only quantum memory [13,14] is recently explored).

Due to the similar transparency phenomenon in EIT and ATS but different applications, distinction between them became an active topic in the past decade [15–21]. For a three-level system there are totally four kinds of types to realize EIT and/or ATS: Λ-, *V*-, upper-driving (where the coupling field drives the middle and upper levels) and lower-driving (where the coupling field drives the middle and lower levels) ladder- (*i.e.* cascade-) types. In 2010 Abi-Salloum theoretically set a threshold to separate EIT from ATS in an unified study of the four kinds of three-level atom systems [15]. The threshold simply replies on decoherence rates of related coupling states (*i.e.* polarization decay rate in Ref. [15]). The author concluded that EIT can

#417529 https://doi.org/10.1364/OE.417529
Journal © 2021 Received 15 Dec 2020; revised 22 Mar 2021; accepted 22 Mar 2021; published 29 Mar 2021

Optics EXPRESS

be observed in only Λ and upper-driving ladder-type systems, while ATS in all four types of three-level atom systems.

In fact, a real physical system is often affected by many experimental parameters. Thus it is necessary and useful to build a EIT-ATS criteria from the lineshape of spectrum obtained experimentally. From this experimental viewpoint, Anisimov *et al.* [16] proposed an objective method based on Akaike information criterion (AIC) to discriminate EIT and ATS, with an additional ability to evaluate their respective weights. Since then this method has been employed and verified in a variety of systems, including Λ-type cold atoms [17], coupled whispering-gallery-mode resonators [18], plasmonic waveguide-resonators coupled system [19], superconducting quantum circuits [20] and coupled mechanical oscillators system [21].

In the field of ladder-type atom system, a Rydberg state is often involved. Motivated by the tunable long-range interactions and special blockade effect between Rydberg atoms, such system has attracted a lot of attentions. There have exhibited numerous applications based on Rydberg-involved EIT effect, such as non-destructive detection of Rydberg state population [22,23], sensitive measurement of microwave electric field [24,25], high resolution imaging of individual particles [26,27], realization of single-photon source [28,29] and single-photon transistor [30–32]. Meanwhile, Rydberg-involved ATS spectroscopy and application have also been investigated [33–40]. Thus distinction of Rydberg-involved EIT and ATS is meaningful for their applications.

Nath *et al.* [41] studied the spectral behaviors of hot atoms, where the upper-driving ladder-type is roughly supposed as EIT spectrum while the lower-driving ladder-type as ATS Spectrum. Further, Hao *et al.* [42] presented the spectrum transition from EIT to ATS in a upper-driving ladder-type cold atoms, where linewidth and transparency window region are respectively used to characterize EIT and ATS. To the best of our knowledge, only Tan *et al.* [43] used AIC method to quantitatively judge the spectral lineshape of Rydberg-involved upper-driving system. We need to notice that their spectra used are theoretically simulations based on hot Rb atoms system in Ref. [22]. In addition, their simulated results (Fig. 6 in Ref. [43]) show only the spectra of EIT-dominated and the EIT-ATS intermediate regions. The absence of ATS-dominated spectrum are attributed to the enhanced absorption by Doppler effect and large wavenumber mismatch between probe and coupling fields.

In this paper, we use AIC method to quantitatively discriminate a series of measured spectra of cold atoms in a Rydberg-involved upper-driving ladder-type configuration. Along Rabi frequency of coupling field increases, the derived weights of EIT and ATS represent that our obtained spectra changes from EIT-ATS intermediate region to ATS-dominated region. The measured weights are compared with the numerically simulated results under ideal conditions. The deviation of measurements from simulation is observed and the influenced factors are analyzed.

2. AIC method

According to Ref. [16], EIT model comprises one broad, positive Lorentzian profile and another narrow, negative Lorentzian one, while the ATS is a sum of two separated Lorentzian profiles. For an ideal three-level system both EIT and ATS have symmetry lineshapes centered at resonant transitions:

$$A_{EIT} = \frac{C_+}{\gamma_+^2/4 + \delta_p^2} - \frac{C_-}{\gamma_-^2/4 + \delta_p^2}, \tag{1}$$

$$A_{ATS} = \frac{C}{\gamma^2/4 + (\delta_p + \delta_0)^2} + \frac{C}{\gamma^2/4 + (\delta_p - \delta_0)^2}, \tag{2}$$

Here C_+, C_-, C are amplitudes of the Lorentzian curves, γ_+, γ_-, γ are their corresponding respective linewidths, δ_p is the frequency detuning of probe field relative to the $|g\rangle$-$|e\rangle$ transition, δ_0 is the shift of ATS peaks.

Optics EXPRESS

However, one spectrum experimentally obtained may have asymmetry lineshape or/and central deviations due to sublevels splitting of multi-level model [17], frequency shift of laser locking and background offset from photodetector. Thus sometimes the ideal EIT and ATS models in Eqs. (1)–(2) need to be revised by adding more parameters [17,20]. Considering asymmetry lineshape and deviations in both horizontal and vertical axes, the profiles of EIT and ATS models can be written as

$$A_{EIT} = \frac{C_+}{\gamma_+^2/4 + (\delta_p - \delta_{eit} - \epsilon)^2} - \frac{C_-}{\gamma_-^2/4 + (\delta_p - \delta_{eit})^2} + y_{eit}, \tag{3}$$

$$A_{ATS} = \frac{C_1}{\gamma_1^2/4 + (\delta_p - \delta_{ats} + \delta_1)^2} + \frac{C_2}{\gamma_2^2/4 + (\delta_p - \delta_{ats} - \delta_2)^2} + y_{ats}, \tag{4}$$

Similarly, C_1 and C_2 are the amplitudes, γ_1, γ_2 are their respective linewidths, δ_{eit}, ϵ, δ_{ats}, δ_1, δ_2 are the shifts from zero frequency. In addition y_{eit} and y_{ats} are the offset from zero absorption.

To quantify the EIT and ATS models, the following expression is employed to calculate their weights [16]:

$$w_{EIT} = \frac{e^{-I_{EIT}/2N}}{e^{-I_{EIT}/2N} + e^{-I_{ATS}/2N}}, w_{ATS} = 1 - w_{EIT}. \tag{5}$$

Here N is the number of spectrum data. I_j (j represents EIT or ATS) quantifies the information lost when model A_j fits actual data and are defined as I_j=-2logL_j+2K_j, where L_j is the maximum likelihood for model A_j with the number of fitting parameters K_j, and can be calculated by the NONLINEARMODELFIT function in MATHMATICA. It is noticed that Ref. [16] also gives an equivalent form of Akaike' information, that is the least-squares analysis I_j=Nlog($\Sigma_1^N \epsilon_k^2/N$), where ϵ_k^2 is the estimated residuals from the fitted model.

3. Experimental setup

Our experiment starts with an standard cold Cs atoms Magneto-Optical Trap (MOT) with a temperature of 100 μK and a peak density of 10^{10} cm^{-3}. The experimental setup is exactly the same as Ref. [42] and further details can also be found in Ref. [44]. From the perspective of structure completeness for this paper, here we still give main procedures and related experimental parameters.

Figure 1 shows the scheme of experimental setup we used. A pair of probe (orange) and coupling (green) beams have linear polarizations in parallel and counter-propagation through a cold Cs atoms cloud. They are overlapped at the center of MOT, with Gaussian waists of ω_p=10 μm and ω_c=30 μm respectively. As shown in the inset, the probe laser couples the transition between ground state $|6S_{1/2}, F = 4\rangle$ (labeled as $|g\rangle$) and intermediate excited state $|6P_{3/2}, F' = 5\rangle$ ($|e\rangle$), while the coupling laser couples the intermediate state and the Rydberg state $|35S_{1/2}\rangle$ ($|R\rangle$). The frequency of probe is locked by polarization spectroscopy [45], while the frequency of coupling laser is stabilized to the $|e\rangle - |R\rangle$ transition by a Rydberg EIT signal obtained from a cesium room-temperature vapor cell [44]. It is noticed that the hyperfine internal of $|R\rangle$ state is estimated to be less than 2 MHz (see Supplement 1), which is on the order of frequency fluctuation of of coupling laser after locking and also the coherent spectroscopy shown below, thus the $|R\rangle$ state is not labeled with hyperfine resolution. The power of probe beam, P_p, is low as 200 pW, inducing that the corresponding Rabi frequency Ω_p=$\mu_{ge}E/\hbar$ = $2\pi\times1.05$ MHz, where μ_{ge} is the matrix element for the dipole transition between coupled states (the data of alkali atoms can be easily calculated by an open software ARC [46]) and the amplitude of probe field E_p has a relationship with P_p by E_P=$\sqrt{2P_p/cn\varepsilon_0\pi\omega_p^2}$. There is similar relationship between the power of coupling beam and its amplitude, allowing convenient change of Rabi frequency of coupling field Ω_c.

Optics EXPRESS

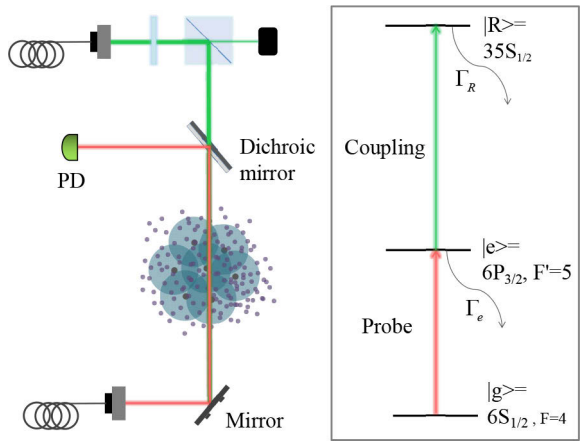

Fig. 1. Scheme of experimental setup. The probe (orange) and coupling (green) beams are counter-propagated and coupled with a cold Cs atoms cloud in a Rydberg-involved upper-driving ladder-type configuration. The relevant three levels are shown in the inset, where Γ_e and Γ_R are the population decay rates of excited and Rydberg states respectively.

In each experimental cycle, after turning off cooling beams of MOT and magnetic field we switch on the coupling and probe beams for 25 μs. During this pulse process the probe laser frequency is swept across $|g\rangle$-$|e\rangle$ transition by using a double-pass acousto-optic modulator (AOM). The EIT or ATS spectral signal is recorded by detecting the transmitted intensity of probe beam with a single-photon counter module (SPCM), followed by a data acquisition card and then processed with a LabVIEW programme. The spectral absorption coefficient, α, is obtained from the SPCM count number P by the relation αL=-ln($P(\delta_p)/P_0$), where P_0 is the count number when probe field is far off resonant (absorption-free) and L the effective diameter of cold atom along the probe beam path.

4. Results

Figures 2(a)-(c) show three typical absorption spectra of ultracold Cs atoms as a function of δ_p with a form of normalized absorption coefficient α. Ω_c in (a-c) is respectively selected to be the minimum, a middle and the maximum values in our obtained spectra with enough signal-noise ratio. They show that the transparency window broadens and transparency dip increases when Ω_c increases. From the spectral lineshape it is hard to evaluate the poles of EIT and ATS by eye, thus some quantatitive analyses based on AIC method are given below.

With all parameters adjustable in Eq. (3) and (4), we fitted the measured spectra with A_{EIT} and A_{ATS} respectively. The fitting results are shown with blue solid lines and red dashes, with derived parameters given in the corresponding caption. These fitting curves give us an impression that EIT model dominates spectrum at low Rabi frequency, while ATS model dominates at high region. Using the form of least-squares in Eq. (5), we plot the measured weights of EIT and ATS in Fig. 2(d) (blue solid and red hollow dots). Each point is averaged with three measurements and the accompanying fittings. It shows that when Rabi frequency of coupling field increases our obtained spectrum varies from EIT-ATS intermediate region to ATS-dominated region. This unobvious difference between EIT-ATS weights is comparative with the obvious difference happening in Λ- type cold atoms system [17,47]. To find out the reasons, we will simulate spectra under the condition of our experimental parameters and calculate their weights.

There has been an standard semiclassical description on the three-level atom systems coupled by two fields, that is Lindblad master equation with population decay rates (*i.e.* natural linewidth)

Optics EXPRESS

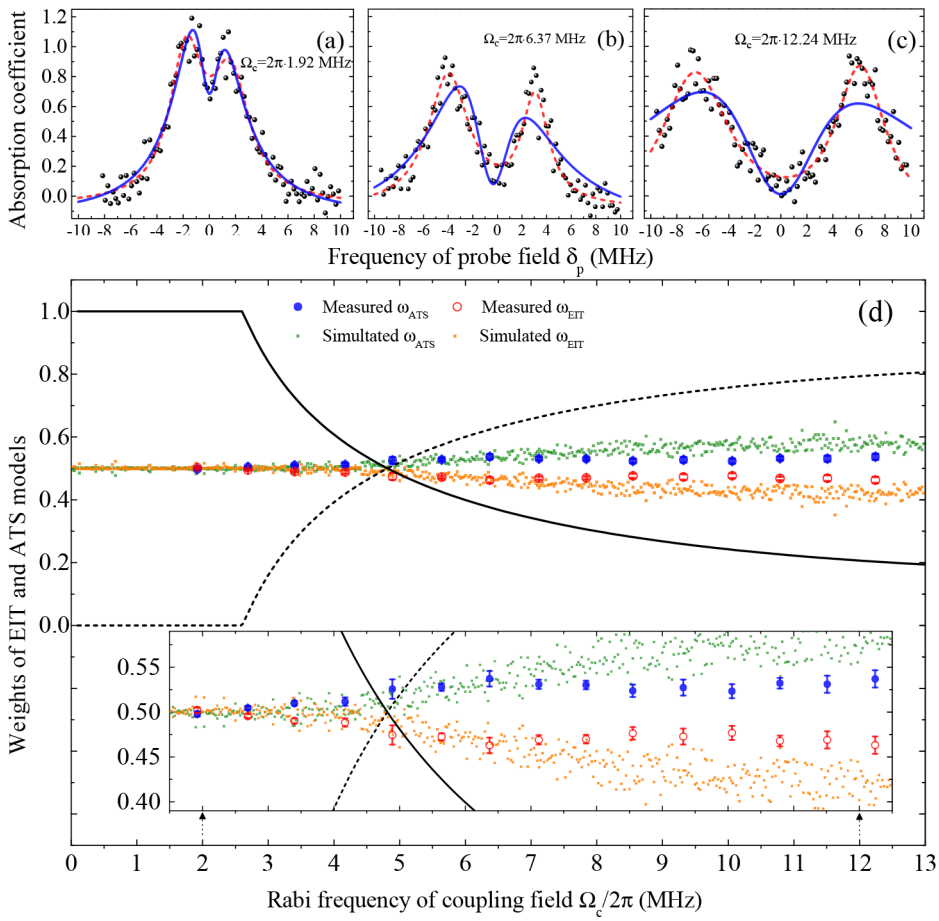

Fig. 2. Absorption spectra of ultracold Cs atoms in our composed Rydberg-involved ladder-type system and the distinctions of EIT and ATS based on AIC method. (a-c) The absorption coefficients as a function of frequency of probe field under three typical Rabi frequencies of coupling fields with values of $2\pi\times1.92$ (a), 6.37 (b) and 12.24 (c) MHz respectively. The blue solid line in each graph is fitting curve with EIT model (Eq. (3)), while the red dash with ATS model (Eq. (4)). The parameters $(C_+, C_-, \gamma_+, \gamma_-, \delta_{eit}, \epsilon, y_{eit})$ in A_{EIT} with best fitting in (a-c) are (25.8, 15.87, 3.60, 2.98, −0.0619, −0.0236, −0.135), (70.44, 43.93, 6.595, 5.331, −0.524, −0.0905, −0.2) and (368.8, 234.2, 14.35, 11.61, −0.144, −0.0663, −0.2) respectively, while the parameters $(C_1, C_2, \gamma_1, \gamma_2, \delta_1, \delta_2, \delta_{ats}, y_{ats})$ in A_{ATS} are (2.273, 2.559, 3.082, 3.549, 1.732, 1.623, −0.0247, −0.0623), (3.687, 1.269, 4.087, 2.662, 4.385, 2.662, 0.402, 0.087) and (10.6, 5.634, 6.531, 4.722, 6.655, 6.064, 0.0587, −0.2) respectively. It needs to be noticed that the offsets of y_{eit} and y_{ats} are limited in the range of [−0.2, 0.2]. (d) Comparison of measured and simulated weights of EIT and ATS models. The weights are derived based on Eq. (5). The blue solid dots and red hollow dots are measured weights of EIT and ATS respectively, while others are simulated results. Among the simulations, the black line and dash are the results under the case of ideal condition, while the green and yellow dots are results in the presence of dephasing rate $\gamma^d_{Rg} = 0.3\Gamma_e$ and the characteristic parameter of Gaussian noise $\sigma = 0.4$ (see contexts below). The inset shows the data zoomed in.

Optics EXPRESS

and dephasing rates manually inserted (for examples, see Refs. [42,48,49]). In our previous work [42] the probe and coupling Rabi frequencies both variety in large ranges, thus we numerically solved Lindblad equation. But here the Rabi frequency of coupling field, Ω_P, is fixed at a value around one over 5 of natural linewidth of state $|e>$, Γ_e ($2\pi\times5.2$ MHz [50]). Under weak field approximation and steady state condition, the density matrix element, ρ_{eg}, which represents the coherence between probe field and the two coupled states, can be obtained as (see *e.g.* Ref. [49])

$$\rho_{eg} = -\frac{i\Omega_p/2}{\gamma_{eg} - i\delta_p + \frac{\Omega_c^2/4}{\gamma_{Rg}-i(\delta_p+\delta_c)}}. \tag{6}$$

Here δ_c is the frequency detuning of coupling field and is set to be zero in the following contexts. γ_{eg}=(Γ_e+Γ_g)/2+γ_{eg}^d, where the linewidth of state $|g>$, Γ_g, is zero. γ_{eg}^d is the dephasing rate between states $|e>$ and $|g>$ and is neglected for that it is much smaller than Γ_e [42,48]. Similarly γ_{Rg}=(Γ_R+Γ_g)/2+γ_{Rg}^d=Γ_R/2+γ_{Rg}^d, where Γ_R is the linewidth of state $|R>$ with a value of $2\pi\times7.02$ kHz (with corresponding lifetime of 22.691 μs [51]), γ_{Rg}^d is the dephasing rate between states $|R>$ and $|g>$. In our previous work [42] γ_{Rg}^d is also be neglected. However, we will see that dephasing rate can not be simply neglected in the contexts below.

Figures 3(a)-(c) show our simulated spectra under several values of γ_{Rg}^d. The spectra are obtained by the imaginary part of Eq. (6). Other parameters have been given before. It is found that both amplitudes of dip and two peaks decrease as γ_{Rg}^d increases. We also notice that the influence on dip is much stronger than the influence on peaks, especially when Ω_c is low. Thus we compare the dip shapes of simulated spectrum and measured one under low Ω_c (*i.e.* Fig. 2(a) and Fig. 3(a)). It looks that the case of $\gamma_{Rg}^d = 0.3\Gamma_e$ matches our measurement better. We attribute the large dephasing rate to the interactions among Rydberg atoms [48].

In the following we show the influence on EIT-ATS models from dephasing rate, we use Eqs. (1)–(2), instead of Eqs. (3)–(4), to fit those spectra in Figs. 3(a)-(c) due to the absolute symmetry of these simulated spectra. For simplify we did not plot their fitting curves and directly plotted the weights of EIT and ATS as a function of Ω_c under different γ_{Rg}^d in Fig. 3(d). It is noticed that here I_j is calculated based on NONLINEARMODELFIT function in MATHMATICA, which is equivalent but simpler than least-squares analysis for simulated spectra. Figure 3(d) shows that there are two tendencies induced by dephasing rate: the crossover from EIT to ATS move to the direction of lower Ω_c, and the difference between EIT and ATS weights increases after crossover. Our measurements shown in Fig. 2(d) agrees with the first tendency, but disagree extremely with the second tendency. We guess that the reason may arise from experimental noise, which has exhibited serious influence in a Λ- type system (*e.g.* see Fig. 3(a) in Ref. [16]).

To see the influence of experimental noise on ladder-type system, we introduce Gaussian noise to the imaginary part of Eq. (6), just like what has been done in Ref. [16]. In detail Imρ_{eg} is converted into (1+ξ)·Imρ_{eg}, where ξ is randomly chosen from the x-axis values of normal distribution exp[-$x^2/\sqrt{2\pi}\sigma$]/$\sqrt{2\pi}\sigma$. ξ represents deviation ratio from an ideal condition without any noise, thus is a mathematical quantification of spectral fluctuation induced by all experimental noises. Figures 4(a)-(c) show the simulated spectra when σ increases from 0.01 to 0.4 in the absence of γ_{Rg}^d while keep other parameters the same as in Figs. 3(a)-(c). It is expected to find that the lineshape has no change and the amplitude fluctuation strengthen as σ increases. Comparing with the spectra in Figs. 2(a)-(c), our experimental noise looks equivalent to the case of σ=0.1~ 0.4. There are many parameters may induce so large noise, such as the frequency uncertainty of probe laser (~MHz [44]) , the fluctuation of atom density, the nonlinear response and uncertainty of AOM voltage controlled oscillator *et al.*.

We then consider the influence of experimental noise on EIT-ATS models. Figure 4(d) plots the weights of EIT and ATS as a function of Ω_c under different σ. The simulation shows that the position of EIT-ATS crossover has no any change but the difference between EIT and ATS weights

Optics EXPRESS

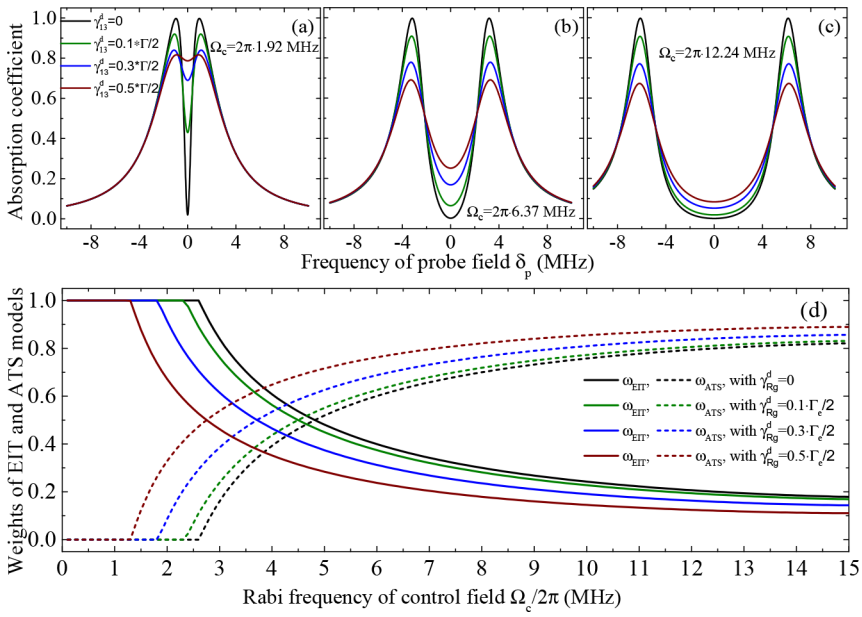

Fig. 3. Simulated absorption spectra (a-c) and the distinctions of EIT and ATS (d) influenced by dephasing rate. The weights of EIT and ATS are obtained by using Eq. (5), in which I_j is calculated based on NONLINEARMODELFIT function in MATHMATICA. The steps of δ_p in (a) and Ω_c in (c) are chosen respectively as 0.05 MHz and 0.1 MHz. The noise characteristic parameter σ are set to be zero (see contexts below). The values of dephasing rate are labeled in graphs.

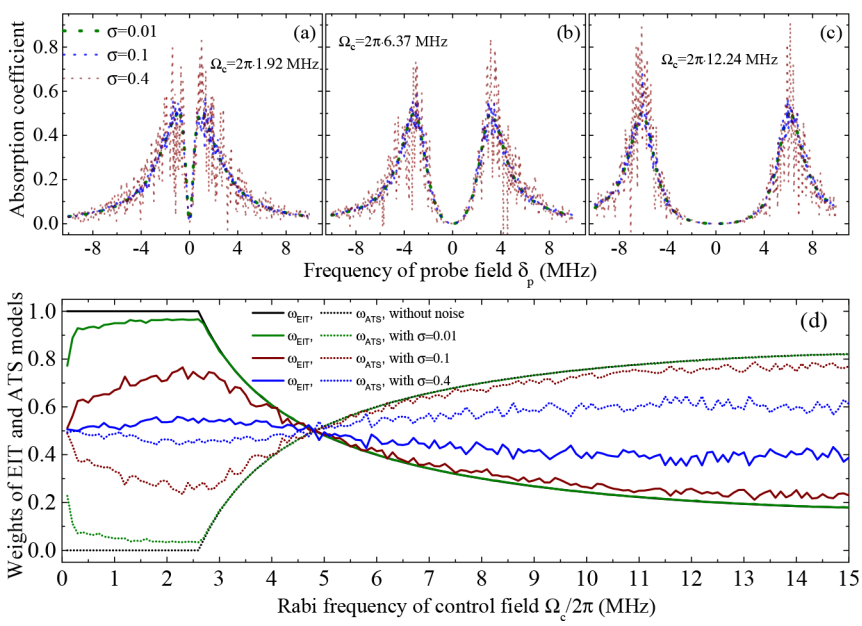

Fig. 4. Simulated absorption spectra (a-c) and the distinctions of EIT and ATS (d) influenced by experimental noise. The standard derivations of Gaussian noise are labeled in graphs. The dephasing rate γ_{Rg}^{d} is set to be zero, while other parameters are the same as in Fig. 3.

Optics EXPRESS

reduces at elsewhere. It is also found that the reduction amplitude is stronger in EIT-dominated range than in ATS-dominated range. This tendency shows that the same amount of noise have different influences on coherence spectroscopy in different region. In EIT-dominated region the noise-induced decoherence strongly weaken the quantum interference mechanism, while in ATS-dominated region only noise-induced disturbances are externally added to the dressed states. If noise is large enough, either EIT model or ATS model is suitable, thus their weights are both equal to 0.5 but with early reach in low EIT-dominated region. Our measurement in Fig. 2(d) is such this situation.

In reality, our measured spectra are affected by the two factors above together. The weights of EIT and ATS based on the simulated spectra with dephasing rate γ_{Rg}^{d}=0.3Γ_e and Gaussian noise σ=0.4 are shown in Fig. 2(d), comparing with the results under ideal condition (in the absence of dephasing rate and experimental noise). It shows that the former simulation agrees better. But there still be some deviation in large range. That is because the acquired spectral region is not large enough when Ω_c is large, inducing incomplete reflection of fitting with ATS model (*e.g.* see the spectrum in Fig. 2(c)).

5. Conclusions

We have demonstrated the distinction of EIT and ATS components by using AIC method in Rydberg-involved upper-driving ladder-type cold atoms. The weights of EIT and ATS reflect that our spectra change from EIT-ATS intermediate region to ATS-dominated region. Our simulations show that there are two factors influencing the spectra in this kind of Rydberg-involved system, that is dephasing rate and experimental noise. The dephasing rate, induced by the interactions among Rydberg atoms, make the dip decreases and make the EIT-ATS crossover move to the direction of low Rabi frequency of coupling field. The experimental noise makes the difference between EIT and ATS weights decreases at elsewhere. By reducing the influences from dephasing rate and experimental noises, one may obtain strong EIT-dominated region at low Rabi frequency of coupling field. Our investigation could provide meaningful reference for the observation and applications of Rydberg-involved quantum coherent spectroscopy.

Funding. National Key Research and Development Program of China (2017YFA0304203); National Natural Science Foundation of China (12034012, 12074231, 61775124, 61835007); NSFC Project for Excellent Research Team (61121064); Fund for Shanxi Key Subjects Construction; PCSIRT (IRT_17R70); Overseas Expertise Introduction Project for Discipline Innovation (D18001).

Acknowledgments. We acknowledge Dr. Jinze Wu for sharing MATHEMATICA programme and helpful discussions.

Disclosures. The authors declare no conflicts of interest.

Data availability. Data underlying the results presented in this paper are not publicly available at this time but may be obtained from the authors upon reasonable request.

Supplemental document. See Supplement 1 for supporting content.

References

1. S. E. Harris, J. E. Field, and A. Imamoğlu, "Nonlinear optical processes using electromagnetically induced transparency," Phys. Rev. Lett. **64**(10), 1107–1110 (1990).
2. K.-J. Boller, A. Imamoğlu, and S. E. Harris, "Observation of electromagnetically induced transparency," Phys. Rev. Lett. **66**(20), 2593–2596 (1991).
3. M. Fleischhauer, A. Imamoglu, and J. P. Marangos, "Electromagnetically induced transparency: Optics in coherent media," Rev. Mod. Phys. **77**(2), 633–673 (2005).
4. U. Fano, "Effects of configuration interaction on intensities and phase shifts," Phys. Rev. **124**(6), 1866–1878 (1961).
5. O. Kocharovskaya, "Amplification and lasing without inversion," Phys. Rep. **219**(3-6), 175–190 (1992).
6. M. Stähler, S. Knappe, C. Affolderbach, W. Kemp, and R. Wynands, "Picotesla magnetometry with coherent dark states," EPL **54**(3), 323–328 (2001).
7. O. Kocharovskaya, Y. Rostovtsev, and M. O. Scully, "Stopping light via hot atoms," Phys. Rev. Lett. **86**(4), 628–631 (2001).

Optics EXPRESS

8. M. D. Lukin, "Colloquium: Trapping and manipulating photon states in atomic ensembles," Rev. Mod. Phys. **75**(2), 457–472 (2003).
9. J. A. Souza, E. Figueroa, H. Chibani, C. J. Villas-Boas, and G. Rempe, "Coherent control of quantum fluctuations using cavity electromagnetically induced transparency," Phys. Rev. Lett. **111**(11), 113602 (2013).
10. S. H. Autler and C. H. Townes, "Stark effect in rapidly varying fields," Phys. Rev. **100**(2), 703–722 (1955).
11. M. A. Quesada, A. M. F. Lau, D. H. Parker, and D. W. Chandler, "Observation of Autler-Townes splitting in the multiphoton ionization of H_2: Measurement of vibronic transition moments between excited electronic states," Phys. Rev. A **36**(8), 4107–4110 (1987).
12. R. Garcia-Fernandez, A. Ekers, J. Klavins, L. P. Yatsenko, N. N. Bezuglov, B. W. Shore, and K. Bergmann, "Autler-Townes effect in a sodium molecular-ladder scheme," Phys. Rev. A **71**(2), 023401 (2005).
13. E. Saglamyurek, T. Hrushevskyi, A. Rastogi, K. Heshami, and L. J. LeBlanc, "Coherent storage and manipulation of broadband photons via dynamically controlled Autler-Townes splitting," Nat. Photonics **12**(12), 774–782 (2018).
14. A. Rastogi, E. Saglamyurek, T. Hrushevskyi, S. Hubele, and L. J. LeBlanc, "Discerning quantum memories based on electromagnetically-induced-transparency and Autler-Townes-splitting protocols," Phys. Rev. A **100**(1), 012314 (2019).
15. T. Y. Abi-Salloum, "Electromagnetically induced transparency and Autler-Townes splitting: Two similar but distinct phenomena in two categories of three-level atomic systems," Phys. Rev. A **81**(5), 053836 (2010).
16. P. M. Anisimov, J. P. Dowling, and B. C. Sanders, "Objectively discerning Autler-Townes splitting from electromagnetically induced transparency," Phys. Rev. Lett. **107**(16), 163604 (2011).
17. L. Giner, L. Veissier, B. Sparkes, A. S. Sheremet, A. Nicolas, O. S. Mishina, M. Scherman, S. Burks, I. Shomroni, D. V. Kupriyanov, P. K. Lam, E. Giacobino, and J. Laurat, "Experimental investigation of the transition between Autler-Townes splitting and electromagnetically-induced-transparency models," Phys. Rev. A **87**(1), 013823 (2013).
18. B. Peng, S. K. Özdemir, W. Chen, F. Nori, and L. Yang, "What is and what is not electromagnetically induced transparency in whispering-gallery microcavities," Nat. Commun. **5**(1), 5082 (2014).
19. L.-Y. He, T.-J. Wang, Y.-P. Gao, C. Cao, and C. Wang, "Discerning electromagnetically induced transparency from Autler-Townes splitting in plasmonic waveguide and coupled resonators system," Opt. Express **23**(18), 23817–23826 (2015).
20. Q.-C. Liu, T.-F. Li, X.-Q. Luo, H. Zhao, W. Xiong, Y.-S. Zhang, Z. Chen, J. S. Liu, W. Chen, F. Nori, J. S. Tsai, and J. Q. You, "Method for identifying electromagnetically induced transparency in a tunable circuit quantum electrodynamics system," Phys. Rev. A **93**(5), 053838 (2016).
21. J. Liu, H. Yang, C. Wang, K. Xu, and J. Xiao, "Experimental distinction of Autler-Townes splitting from electromagnetically induced transparency using coupled mechanical oscillators system," Sci. Rep. **6**(1), 19040 (2016).
22. A. K. Mohapatra, T. R. Jackson, and C. S. Adams, "Coherent optical detection of highly excited Rydberg states using electromagnetically induced transparency," Phys. Rev. Lett. **98**(11), 113003 (2007).
23. J. D. Pritchard, D. Maxwell, A. Gauguet, K. J. Weatherill, M. P. A. Jones, and C. S. Adams, "Cooperative atom-light interaction in a blockaded Rydberg ensemble," Phys. Rev. Lett. **105**(19), 193603 (2010).
24. Y. Jing, Mingyongand Hu, J. Ma, H. Zhang, L. Zhang, L. Xiao, and S. Jia, "Atomic superheterodyne receiver based on microwave-dressed Rydberg spectroscopy," Nat. Phys. **16**(9), 911–915 (2020).
25. J. A. Sedlacek, A. Schwettmann, H. Kübler, R. Löw, T. Pfau, and J. P. Shaffer, "Microwave electrometry with Rydberg atoms in a vapour cell using bright atomic resonances," Nat. Phys. **8**(11), 819–824 (2012).
26. C. Gross, T. Vogt, and W. Li, "Ion imaging via long-range interaction with Rydberg atoms," Phys. Rev. Lett. **124**(5), 053401 (2020).
27. G. Günter, M. Robert-de Saint-Vincent, H. Schempp, C. S. Hofmann, S. Whitlock, and M. Weidemüller, "Interaction enhanced imaging of individual Rydberg atoms in dense gases," Phys. Rev. Lett. **108**(1), 013002 (2012).
28. T. Peyronel, O. Firstenberg, Q.-Y. Liang, S. Hofferberth, A. V. Gorshkov, T. Pohl, M. D. Lukin, and V. Vuletić, "Quantum nonlinear optics with single photons enabled by strongly interacting atoms," Nature **488**(7409), 57–60 (2012).
29. Y. O. Dudin and A. Kuzmich, "Strongly interacting Rydberg excitations of a cold atomic gas," Science **336**(6083), 887–889 (2012).
30. Y. M. Yao, G. W. Lin, X. M. Lin, Y. P. Liu, and S. Q. Gong, "Single-photon transistor based on cavity electromagnetically induced transparency with Rydberg atomic ensemble," Sci. Rep. **9**(1), 4723 (2019).
31. H. Gorniaczyk, C. Tresp, J. Schmidt, H. Fedder, and S. Hofferberth, "Single-photon transistor mediated by interstate Rydberg interactions," Phys. Rev. Lett. **113**(5), 053601 (2014).
32. D. Tiarks, S. Baur, K. Schneider, S. Dürr, and G. Rempe, "Single-photon transistor using a Förster resonance," Phys. Rev. Lett. **113**(5), 053602 (2014).
33. B. K. Dutta and P. K. Mahapatra, "Nonlinear optical effects in a doubly driven four-level atom," Phys. Scr. **75**(3), 345–353 (2007).
34. D. A. Anderson, A. Schwarzkopf, S. A. Miller, N. Thaicharoen, G. Raithel, J. A. Gordon, and C. L. Holloway, "Two-photon microwave transitions and strong-field effects in a room-temperature Rydberg-atom gas," Phys. Rev. A **90**(4), 043419 (2014).
35. H. Zhang, L. Zhang, L. Wang, S. Bao, J. Zhao, S. Jia, and G. Raithel, "Autler-Townes spectroscopy with interaction-induced dephasing," Phys. Rev. A **90**(4), 043849 (2014).

Optics EXPRESS

36. H. Zhang, L. Wang, J. Chen, S. Bao, L. Zhang, J. Zhao, and S. Jia, "Autler-Townes splitting of a cascade system in ultracold cesium Rydberg atoms," Phys. Rev. A **87**(3), 033835 (2013).
37. B. J. DeSalvo, J. A. Aman, C. Gaul, T. Pohl, S. Yoshida, J. Burgdörfer, K. R. A. Hazzard, F. B. Dunning, and T. C. Killian, "Rydberg-blockade effects in Autler-Townes spectra of ultracold strontium," Phys. Rev. A **93**(2), 022709 (2016).
38. B. K. Teo, D. Feldbaum, T. Cubel, J. R. Guest, P. R. Berman, and G. Raithel, "Autler-Townes spectroscopy of the $55S_{1/2}$-$5P_{3/2}$-44D cascade of cold ^{85}Rb atoms," Phys. Rev. A **68**(5), 053407 (2003).
39. M. J. Piotrowicz, C. MacCormick, A. Kowalczyk, S. Bergamini, I. I. Beterov, and E. A. Yakshina, "Measurement of the electric dipole moments for transitions to rubidium Rydberg states via Autler-Townes splitting," New J. Phys. **13**(9), 093012 (2011).
40. J. Bai, J. Wang, S. Liu, J. He, and J. Wang, "Autler-Townes doublet in single-photon Rydberg spectra of cesium atomic vapor with a 319 nm UV laser," Appl. Phys. B **125**(3), 33 (2019).
41. S. K. Nath, V. Naik, A. Chakrabarti, and A. Ray, "Discriminating electromagnetically induced transparency from Autler-Townes splitting in a Ξ system," J. Opt. Soc. Am. B **36**(9), 2610–2617 (2019).
42. L. Hao, Y. Jiao, Y. Xue, X. Han, S. Bai, J. Zhao, and G. Raithel, "Transition from electromagnetically induced transparency to Autler-Townes splitting in cold cesium atoms," New J. Phys. **20**(7), 073024 (2018).
43. C. Tan and G. Huang, "Crossover from electromagnetically induced transparency to Autler-Townes splitting in open ladder systems with Doppler broadening," J. Opt. Soc. Am. B **31**(4), 704–715 (2014).
44. Y. Jiao, J. Li, L. Wang, H. Zhang, L. Zhang, J. Zhao, and S. Jia, "Laser frequency locking based on Rydberg electromagnetically induced transparency," Chin. Phys. B **25**(5), 053201 (2016).
45. C. P. Pearman, C. S. Adams, S. G. Cox, P. F. Griffin, D. A. Smith, and I. G. Hughes, "Polarization spectroscopy of a closed atomic transition: applications to laser frequency locking," J. Phys. B: At., Mol. Opt. Phys. **35**(24), 5141–5151 (2002).
46. N. Šibalić, J. D. Pritchard, C. S. Adams, and K. J. Weatherill, "ARC: An open-source library for calculating properties of alkali Rydberg atoms," Comput. Phys. Commun. **220**, 319–331 (2017).
47. X.-G. Lu, X.-X. Miao, J.-H. Bai, Y. Yuan, L.-A. Wu, P.-M. Fu, R.-Q. Wang, and Z. Zhan-Chun, "Crossover between electromagnetically induced transparency and Autler-Townes splitting with dispersion," Chin. Phys. B **24**(9), 094204 (2015).
48. U. Raitzsch, R. Heidemann, H. Weimer, B. Butscher, P. Kollmann, R. Löw, H. P. Büchler, and T. Pfau, "Investigation of dephasing rates in an interacting Rydberg gas," New J. Phys. **11**(5), 055014 (2009).
49. J. Gea-Banacloche, Y.-Q. Li, S.-Z. Jin, and M. Xiao, "Electromagnetically induced transparency in ladder-type inhomogeneously broadened media: Theory and experiment," Phys. Rev. A **51**(1), 576–584 (1995).
50. D. A. Steck, "Cesium D Line Data," available online at http://steck.us/alkalidata (revision 2.2.1, 21 November 2019).
51. I. I. Beterov, I. I. Ryabtsev, D. B. Tretyakov, and V. M. Entin, "Quasiclassical calculations of blackbody-radiation-induced depopulation rates and effective lifetimes of Rydberg nS, nP, and nD alkali-metal atoms with $n \leq 80$," Phys. Rev. A **79**(5), 052504 (2009).